International Immunopharmacology 124 (2023) 110984

Contents lists available at ScienceDirect

International Immunopharmacology

journal homepage: www.elsevier.com/locate/intimp

Linderalactone mitigates diabetic cardiomyopathy in mice via suppressing the MAPK/ATF6 pathway

Xue Han [a,b,c,1], Wenwei Zhou [b,1], Jiajia Zhang [b], Yu Tu [b], Jiajia Wei [b], Ruyi Zheng [b], Jian Zhu [d], Diyun Xu [a], Huazhong Ying [b,d], Gaojun Wu [a,*], Qiaojuan Shi [b,*], Guang Liang [a,c,*]

[a] Department of Cardiology, The First Affiliated Hospital of Wenzhou Medical University, Wenzhou, Zhejiang 325035, China
[b] Zhejiang Provincial Key Laboratory of Laboratory Animals and Safety Research, Hangzhou Medical College, Hangzhou 310013, China
[c] Chemical Biology Research Center, School of Pharmaceutical Sciences, Wenzhou Medical University, Wenzhou, Zhejiang 325035, China
[d] College of Pharmaceutical Science, Zhejiang Chinese Medical University, Hangzhou 310053, China

ARTICLE INFO

Keywords:
Diabetic cardiomyopathy
Linderalactone
MAPK
ATF6
Endoplasmic reticulum stress
Inflammation

ABSTRACT

Diabetic cardiomyopathy (DCM) is a challenging diabetic complication that manifests as chronic inflammation. Yet, the mechanism underlying diabetes-associated myocardial injury is not fully understood. We investigated the pharmacological effects and mechanisms of linderalactone, a natural compound that can prevent diabetes-induced cardiomyopathy in mice. Diabetes was induced by a single dose of streptozotocin (120 mg/kg, *i.p.*). Diabetic mice were administrated with linderalactone (2.5 or 5 mg/kg) by gavage for five weeks. Harvested heart tissues were then subjected to RNA-sequencing analysis to explore the potential mechanism of linderalactone. Linderalactone prevented heart dysfunction by inhibiting myocardial hypertrophy, fibrosis, and inflammation, without altering blood glucose. RNA-sequencing indicated that linderalactone exerted its cardioprotective effects mainly by affecting the mitogen-activated protein kinase (MAPK)/ activating transcription factor 6 (ATF6) pathway. Linderalactone also suppressed endoplasmic reticulum (ER) stress mediated by the diabetes-activated MAPKs/ATF6 pathway, thereby reducing myocardial hypertrophy and inflammation in heart tissues and in cultured cardiomyocytes. Inhibition of MAPKs or a deficiency of ATF6 in cardiomyocytes mimicked the linderalactone-associated decreases in high glucose-induced hypertrophy and inflammation. Linderalactone showed beneficial effects in alleviating diabetic cardiomyopathy, in part by modulating the MAPK/ATF6 signaling pathway to mitigate myocardial hypertrophy and inflammation. Linderalactone may have clinical utility in the treatment for diabetes-associated cardiomyopathy.

1. Introduction

Diabetes mellitus (DM) patients are vulnerable to the development of ventricular remodeling and even heart failure [1]. DM induces myocardial structural abnormalities and left ventricular dysfunction, independent of other traditional risk factors such as hypertension, atherosclerosis and coronary heart disease, in a process termed diabetic cardiomyopathy (DCM) [2]. Nearly half of asymptomatic/normotensive patients with well-controlled DM have myocardial lesions [3]. Currently, DCM has no specific therapy other than the application of renin-angiotensin system inhibitors and lowering blood glucose and lipid levels [4]. Therefore, depth elucidation of the pathological mechanisms of DCM and discovery of better pharmacological interventions are urgently needed.

The progression of DCM has been associated with several pathophysiological factors, including myocardial inflammation, apoptosis, fibrosis, mitochondrial dysfunction, and endoplasmic reticulum (ER) stress [5]. Among these causes, chronic inflammation seems to be a critical event that induces cardiomyocyte impairment. Increases in several inflammatory cytokines, including interleukin-6 (IL-6), IL-1β and tumor necrosis factor-α (TNF-α), have been found in both diabetic patients and diabetic animal models and can result in excessive tissue

* Corresponding authors at: Department of Cardiology, the First Affiliated Hospital of Wenzhou Medical University, Wenzhou, Zhejiang 325035, China (Guang Liang). Zhejiang Provincial Key Laboratory of Laboratory Animals and Safety Research, Hangzhou Medical College, Hangzhou 310013, China (Qiaojuan Shi). First Affiliated Hospital of Wenzhou Medical University, Wenzhou, Zhejiang 325035, China (Gaojun Wu).
E-mail addresses: gaojunwuwyyy@163.com (G. Wu), shiqiaojuan@163.com (Q. Shi), wzmcliangguang@163.com (G. Liang).
[1] These authors contributed equally to this work.

https://doi.org/10.1016/j.intimp.2023.110984
Received 12 July 2023; Received in revised form 17 September 2023; Accepted 21 September 2023
Available online 25 September 2023

remodeling, and eventual progression to cardiac fibrosis and tissue stiffness [6]. The most widely described inflammatory cascades involved in the development of DCM are initiated by the mitogen-activated protein kinase (MAPK) signaling pathway [7]. Activation of the MAPK members c-Jun N-terminal kinase (JNK), extracellular-regulated protein kinase (Erk), and p38 are known to occur under diabetic conditions, and are involved in cardiac hypertrophy, fibrosis and inflammation [8]. By contrast, inhibition of MAPK activation can ameliorate the adverse effects of DCM [9,10]. Therefore, the MAPK pathway may be a strategic therapeutic target for improving the cardiomyopathy associated with diabetes. One potential source of new therapeutic agents is traditional medicine derived from natural products.

An accumulating number of preclinical studies now favour the use of herbal medicines, such as triptolide [11], curcumin [12] and myricitrin [13], as possible therapies for DCM. One compound showing promise as a DCM treatment is linderalactone, a sesquiterpene lactone isolated from root extracts of *Lindera aggregata* [14,15]. This compound can suppress the activity of several types of cancer cells [16], suggesting that it has appreciable pharmacological potential. For example, linderalactone inhibits the growth of A549 lung cancer cells by inducing apoptosis and suppressing the JAK/STAT signaling pathway [16]. Evidence also displays that linderalactone can inhibit the enzymatic activity of α-glucosidase with an IC_{50} value of 12.72 μM [14]. However, the possible effects of linderalactone treatment on diabetes-associated cardiac dysfunction have not been investigated.

In the present study, we examined the effects of a five-week linderalactone treatment on the streptozotocin (STZ)-induced diabetic mouse model. We found that linderalactone administration alleviated cardiac dysfunction, hypertrophy and fibrosis caused by diabetes indicating that its therapeutic effect in the progression of DCM. Mechanistically, linderalactone suppressed MAPK/ATF6 signaling pathway which plays important role in promoting intracellular inflammation and endoplasmic reticulum in cardiomyocytes This finding identified linderalactone as a novel agent for diabetic cardiomyopathy.

2. Materials and methods

2.1. Animals

Eight-week-old male C57BL/6 mice weighing 18–22 g were obtained from the Laboratory Animal Center of Hangzhou Medical College (Hangzhou, China). The animals were housed under a light–dark cycle of 12 h in plastic cages at 22℃ with 40–60% humidity and provided with food and water ad libitum. All experimental procedures were carried out in strict accordance with the National Institutes of Health Guidelines for the Care and the Use of Laboratory Animals and the study was approved by the Ethics Committee of Laboratory Animal Care and Welfare, Zhejiang Center of Laboratory Animals (Approval Number: ZJCLA-IACUC-20040066; Approval date: April 3, 2021). All efforts were made to reduce the number of animals and minimize their suffering.

2.2. Experimental design

Type 1 DM (T1DM) was induced with a single intraperitoneal injection of STZ (Sigma-Aldrich, St. Louis, MO, United States) at a dose of 100 mg/kg formulated in 100 mM citrate buffer (pH 4.5) as previously described [17]. Control animals received citrate buffer alone on the same regimen. One week later, blood glucose levels were measured utilizing a glucometer from collected caudal vein blood. Animals with fasting blood glucose over 12 mmol/L were considered as DM and were used for the further study. The STZ-induced diabetic mice were randomly allocated into three experimental groups (n = 7 per group): a vehicle control group (0.5% carboxymethylcellulose-Na solution), a low-dose linderalactone group (2.5 mg/kg; the chemical structure was shown in Fig. 1A; purity, ≥ 98.0%; MedChemExpress, Bloomfield, NJ, USA), and a high-dose linderalactone group (5 mg/kg). Linderalactone was administered every other day for 5 weeks by gavage. The corresponding control groups received vehicle for the same duration. At the desired time points, blood glucose and body weight were measured. After the 5-week administration, mice were anaesthetized with 40 mg/kg body weight phenobarbital sodium (*i.p.*). Blood samples were collected and centrifuged at 4℃ at 3000 rpm for 10 min to collect serum for lactate dehydrogenase (LDH) and creatine kinase-MB (CK-MB) determinations. Heart tissues and tibia length were measured, and heart tissues were embedded in 4% paraformaldehyde or snap-frozen in liquid nitrogen for further analysis (Fig. 1B).

2.3. Cardiac function evaluation

One day before sacrifice, transthoracic echocardiography was performed to evaluate systolic and diastolic cardiac function. The mice were anaesthetized with 1.0% isoflurane, placed supinely on a heating platform and analyzed using a Vevo 2100 High-Resolution Micro-Ultrasound System (FUJIFILM Visual Sonics, Toronto, ON, Canada). The ejection fraction (EF) was calculated from the LV end-diastolic volume (LVEDV) and end-systolic volume (LVESV) using the equation (EF% = [(LVEDV - LVESV)/LVEDV] × 100%). Fractional shortening (FS) was calculated using the equation (FS% = [(LVIDd - LVIDs)/LVIDd] × 100%).

2.4. Histomorphology

Heart tissues were immersed in 4% paraformaldehyde at room temperature for 48 h, and then embedded in paraffin. The embedded tissues were cut into 5-μm-thick sections and stained with haematoxylin and eosin (H&E), Masson's trichrome, or Sirius red for pathological analysis. The stained sections were then observed under a light microscope (magnification: 200×; Leica Microsystems, Wetzler, HE, Germany). The relative positive areas of Masson's trichrome and Sirius red staining were analyzed using Image-Pro Plus software (Media Cybernetics, Silver Spring, MD, USA) under "Analyze-Measure" module. Seven mice in each group and 2 sections per mouse were used for the above staining, and 5 random fields in each section were captured by an investigator who was blind to the treatment. The average positive areas (%) = (positive area/total area) × 100.

2.5. RNA-sequencing analysis

Total RNA extracted from heart tissues was submitted for RNA sequencing. The total RNA was isolated using TRIzol Reagent (Invitrogen, Carlsbad, CA, USA) according to the manufacturer's procedure. The RNA amount and purity were evaluated and quantified for each heart sample using a NanoDrop ND-1000 instrument (NanoDrop, Wilmington, DE, USA) and an Agilent 2100 bioanalyzer (Thermo Fisher Scientific, Waltham, MA, USA). RNA integrity was confirmed by electrophoresis on a denaturing agarose gel. Oligo(dT)-attached magnetic beads were used to purify the mRNA, which was then fragmented into small pieces with a fragmenting buffer at an appropriate temperature. The cleaved RNA fragments were then reverse-transcribed into cDNA using random hexamer-primed reverse transcription. Subsequently, A-Tailing Mix and RNA Index Adapters were added and incubated to promote end repair. Sequence analysis was then performed on the BGISEQ-500 platform (Beijing Genomics Institute, Shenzhen, China).

Bowtie2 (v2.2.5) and HISAT2 (v2.0.4) were used to map the clean reads to the reference gene and genome, respectively. The gene expression level (FPKM) was quantified using RSEM (v1.2.12). Differentially expressed genes (DEGs) were selected using the following criterion: fold change > 2 and p-value < 0.05 or fold change < 0.5 and p-value < 0.05. Pathway enrichment analysis was performed by using the public Kyoto Encyclopedia of Genes and Genomes (KEGG) database (https://www.kegg.jp/). The analysis of potential transcription factors for the DEGs was based on TRRUST (Version 2) database in Enrichr

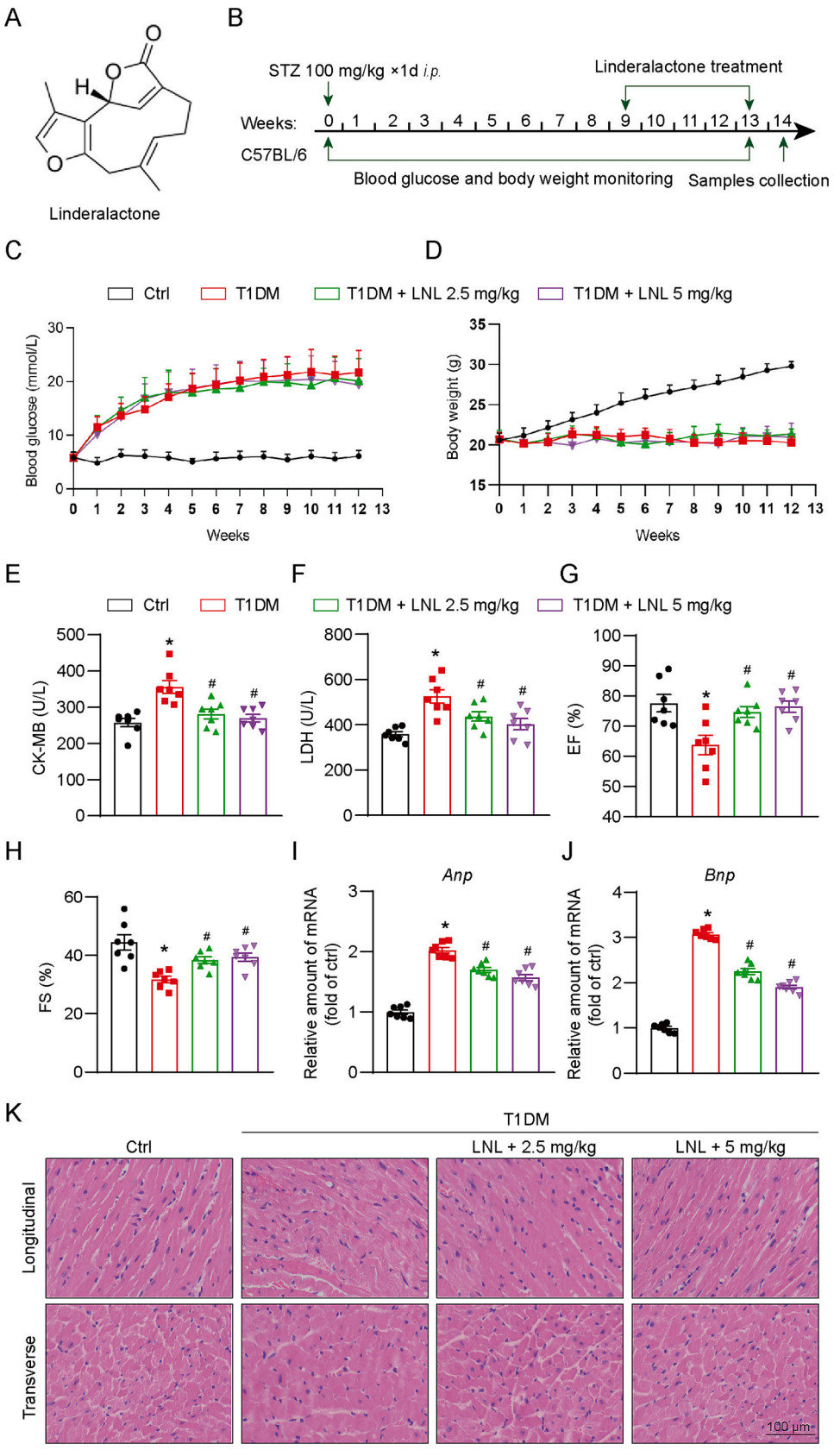

(caption on next page)

Fig. 1. Linderalactone attenuates cardiac pathological changes and hypertrophy in T1DM mice. (A) The chemical structure of linderalactone. (B) Illustration of experimental schedule. Mice were intraperitoneal injected with 100 mg/kg STZ to induce T1DM model, and injected with citrate buffer as control group. The blood glucose and body weight of mice were monitored every week. T1DM mice were treated with linderalactone (5 mg/kg/day and 10 mg/kg/day, *i.g.*) from 9th week to 13th week. After 5 weeks treatment, blood and heart tissues were collected. Linderalactone treatment did not modify the blood glucose (C) or body weight (D) in diabetic mice. (E, F) Serum levels of CK-MB and LDH in mice were determined. (G, H) The ejection fraction (EF) values and fractional shortening (FS) values of mice were measured by ultrasonic scanning image system. (I, J) The mRNA expression levels of *Anp* and *Bnp* in the myocardial tissues were detected by RT-qPCR. (k) Representative H&E staining image of heart tissues. Scale bar, 100 μm. Values are mean ± SEM, (n = 7 per group). $^{*}P < 0.05$ versus control; $^{\#}P < 0.05$ versus T1DM. Ctrl, control; T1DM, type 1 diabetes mellitus; STZ, streptozotocin; LNL, linderalactone.

website (https://maayanlab.cloud/Enrichr/).

2.6. Cell culture and treatment

The embryonic rat heart-derived H9C2 cell line was purchased from the Shanghai Institute of Biochemistry and Cell Biology (Shanghai, China). The H9C2 cells were maintained at 37℃ with 5% CO_2 and 95% O_2 in Dulbecco's modified Eagle medium (DMEM; Gibco, Eggenstein, BW, Germany) containing 5.5 mM D-glucose supplemented with 10% fetal bovine serum (FBS; Hyclone, UT, USA), 100 U/mL penicillin, and 100 μg/mL streptomycin. For the linderalactone (Selleck Chemicals, Houston, TX, USA) treatment, linderalactone was dissolved in dimethyl sulfoxide (DMSO). The other groups received equivalent volumes of DMSO. The H9C2 cardiomyocytes were pre-treated with 10 μM or 20 μM linderalactone for 1 h. Cells in high-glucose group were maintained in DMEM containing 27.5 mM D-glucose (total 33 mM; Sigma-Aldrich) for 24 h. Control cells were maintained in DMEM containing 5.5 mM D-glucose. For MAPK inhibitory assays, a mixture of MAPKs inhibitors (JNK inhibitor, SP600125, 5 μM; ERK inhibitor, U0126, 5 μM; p38 inhibitor, SB230580, 5 μM; Sigma-Aldrich) was added 1 h prior to the linderalactone treatment.

2.7. Cardiomyocyte staining

Hypertrophic changes were observed by fixing H9C2 cells were fixed with 4% paraformaldehyde permeabilizing with 0.1% Triton-X100 and staining with rhodamine phalloidin (50 μg/mL; Beyotime, Shanghai, China) for 60 min at room temperature. Nuclei were stained with DAPI for 10 min at room temperature. Images were viewed and captured using fluorescence microscope (200 × amplification; Leica Microsystems). Each group stained for 3 slides, and each slide randomly captured 5 nonoverlapping images. > 10 cell areas in each slide were analyzed using Image-Pro Plus software (Media Cybernetics), and the average cell area = total cell areas/cell number.

For calcium flux analysis, H9C2 cells were incubated with 2 μM Fluo-4-AM (Thermo Fisher Scientific) at 37℃ for 30 min and then washed with phosphate buffered saline and observed by fluorescence microscope (200 × amplification, Leica Microsystems).

2.8. RNA interference

Small interfering RNA (siRNA) targeting rat activating transcription factor 6 (ATF6) was synthesized by Gene Pharma Co. Ltd. (Shanghai, China): sense: GGGACUAUGAGGAGAUGAUTT, antisense: AUCAUCUCCUCAUAGUCCCTT. The siRNA molecules (50 nM) were mixed with Lipofectamine™ 2000 (5 μL; Thermo Fisher Scientific) in serum-free Opti-MEM™ (250 μL; Thermo Fisher Scientific) and incubated at room temperature for 20 min. The mixture was added to H9C2 cells in DMEM containing FBS but lacking antibiotics and incubated for 24 h. The transfection efficiency was determined based on the protein and mRNA levels.

2.9. Real-time quantitative PCR (RT-qPCR)

Total RNA was extracted from cells and tissues using TRIzol (Invitrogen). Reverse transcription and quantitative PCR were performed using Hifair III 1st Strand cDNA Synthesis SuperMix (YEASEN, Shanghai, China), and Hieff UNICON qPCR SYBR Green Master Mix (YEASEN). RT-qPCR was carried out using a BioRad CFX96 TouchTM Real-Time PCR Detection System (BioRad, Hercules, California, USA). Primers for genes including atrial natriuretic peptide (*Anp*), brain natriuretic peptide (*Bnp*), transforming growth factor-β (*Tgfβ1*), collagen type 1 (*Col1*), *Tnf-α*, *Il6* and β-actin genes were synthesized in Sangon Biotech (Shanghai, China), as listed in the Supplementary Table S1. Gene expression was normalized based on the level of β-actin RNA expression. All samples were determined in duplicate.

2.10. Flow cytometry

Annexin V and PI apoptosis kits (Beyotime) were applied for evaluation of cell death. After harvested of H9C2 cells, the binding buffer with FITC and PI were used to incubate cells for 15 min in dark circumstances. Flow cytometry was performed to assess cell death. The annexin V-positive cells and PI-negative cells (early apoptosis), and annexin V-positive cells and PI-positive cells (late apoptosis) were regarded as death cells.

2.11. Immunoblotting

Cells and heart tissue samples were homogenized and lysed using a cell and tissue total protein extraction kit (Kang Cheng Bioengineering, Shanghai, China). Protein samples were measured with a BCA protein assay kit (Beyotime) and then separated on SDS-PAGE gels and electrotransferred to poly vinylidene fluoride membranes. Membranes were blocked for 1 h at room temperature with 5% non-fat milk or 5% BSA at room temperature. Membranes were then incubated with various primary antibodies overnight at 4℃. Antibodies for phospho-JNK (Cat. NO. 9255, 1:1000), JNK (Cat. NO. 9252, 1:1000), phospho–p38 (Cat. NO. 4511, 1:1000), cleaved-casepase 3 (Cat. NO. 9662, 1:1000), casepase 3 (Cat. NO. 9664 s, 1:2000) and Chop (Cat. NO. 2895, 1:1000) were obtained from Cell Signaling Technology (Topsfield, MA, USA). Antibodies for p38 (Cat. NO. 14064–1-AP,1:1000), phospho–ERK1/2 (Cat. NO. 28733–1-AP, 1:1000), ERK1/2 (Cat. NO. 16433–1-AP, 1:1000), Bcl-2 (Cat. NO. 12789–1-AP, 1:1000), ATF6 (Cat. NO. 24169–1-AP, 1:1000) and GAPDH (Cat. NO. 60004–1-Ig, 1:1000) were purchased from Proteintech (Wuhan, Hubei, China). Immunoreactive bands were detected by incubating with secondary antibodies conjugated to horseradish peroxidase (1:3000; Servicebio, Wuhan, Hubei, China) for 2 h at room temperature, followed by treatment with an ECL chemiluminescence kit. The band density was calculated using Image J software (NIH, Bethesda, MD, USA) and normalized to GAPDH as the internal control.

2.12. Statistics

All data were collected from at least three independent experiments and were presented as means ± SEMs. Statistical analyses were performed using GraphPad Pro Prism 8.01 (GraphPad, CA, USA). One-way ANOVA, followed by Tukey's multiple comparisons test, was employed to assess the differences between the groups. Differences were considered statistically significant at P value < 0.05.

3. Results

3.1. Linderalactone prevents DCM in T1DM mice

To explore the potential effect of linderalactone on DCM, the T1DM mice were administrated with linderalactone (2.5 or 5 mg/kg) on alternate days over 5 weeks. The T1DM mice exhibited increased blood glucose levels and decreased body weight compared with the control group. By contrast, T1DM mice administrated linderalactone showed no changes in these two indexes when compared to untreated T1DM mice (Fig. 1C, D). Serum markers of myocardial cellular damage, including CK-MB and LDH, were significantly elevated in T1DM mice compared with the control group, and linderalactone treatment prevented these increases (Fig. 1E, F, $P < 0.05$). Estimations of cardiac function using echocardiography showed that linderalactone significantly improved cardiac systolic and diastolic dysfunction in diabetic mice, as evidenced by increases in the EF% and FS%, and decreases in the LVIDd and IVSD (Fig. 1G, H, Table S2, $P < 0.05$). The elevated mRNA levels of *Anp* and *Bnp* were also significantly reduced by linderalactone in diabetic heart tissues (Fig. 1I, J, $P < 0.05$). In addition, linderalactone treatment significantly decreased T1DM-induced the increased ratio of heart weight to tibia length (Table S2, $P < 0.05$). Similarly, H&E staining showed obviously structural and hypertrophic alterations in T1DM mice, but not in mice administration of linderalactone (Fig. 1K). These results suggest that linderalactone protects against diabetes-induced cardiac dysfunction and pathological changes in T1DM mice.

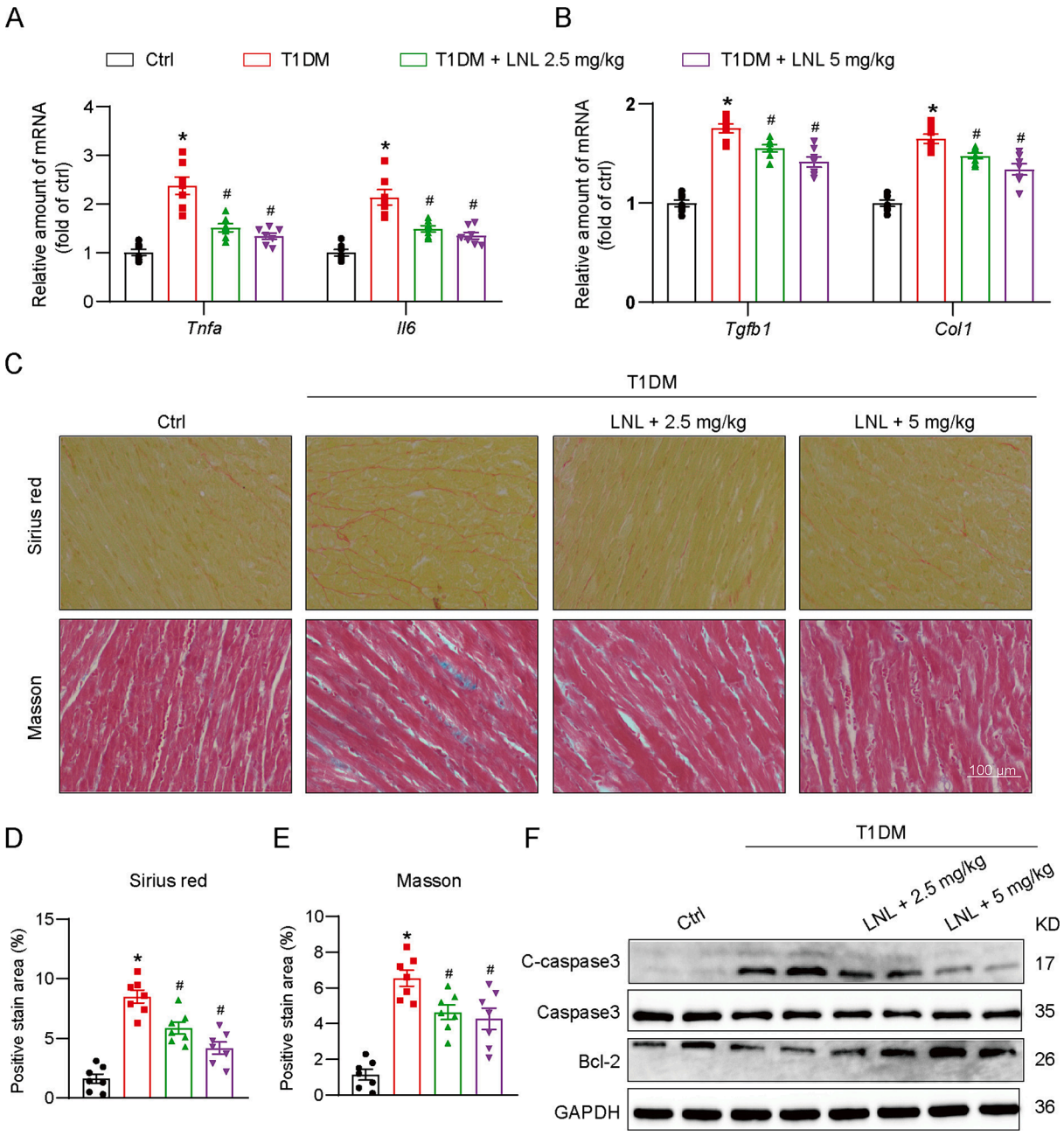

Fig. 2. Linderalactone protects against diabetic-induced inflammation, fibrosis and apoptosis in heart tissues. (A, B) The mRNA levels of *Tnfa*, *Il6*, *Tgfb1* and *Col1* in the heart tissues. Transcripts were normalized to *Actb*. (C) Representative images for Sirius red staining and Masson staining in the heart tissues. Scale bar, 100 μm. Quantification analysis of Sirius red staining (D) and Masson staining (E). (F) Western blot analysis of cleaved caspase-3, Caspase-3 and Bcl-2 in the myocardial tissues. GAPDH was used as the loading control. Values are mean ± SEM, (A-E: n = 7 per group; F: n = 4 per group). $^{*}P < 0.05$ versus control; $^{\#}P < 0.05$ versus T1DM. Ctrl, control; T1DM, type 1 diabetes mellitus; LNL, linderalactone.

3.2. Linderalactone protects against diabetes-induced inflammation, fibrosis and apoptosis in heart tissues

Compared to control mice, T1DM mice exhibited increased mRNA levels of *Tnfa, Il6, Tgfb1* and *Col1* in heart tissues (Fig. 2A, B, $P < 0.05$). Consistent with the RT-qPCR results, Sirius red and Masson's trichrome staining also showed distinctly fibrotic areas in T1DM mouse heart tissues (Fig. 2C-E). While linderalactone treatment significantly mitigated these unfavorable changes (Fig. 2A-E, $P < 0.05$), and also downregulating the diabetic-induced the activation of apoptosis-related proteins, including cleaved-caspase3 and bcl-2 in diabetic heart tissues (Fig. 2F, Supplementary Fig. S1A, $P < 0.05$). These results indicate that linderalactone prevents diabetes-induced inflammation, fibrosis and apoptosis in mice.

3.3. Linderalactone inhibits diabetes-induced MAPK activation and mitigates ATF6-mediated endoplasmic reticulum stress in T1DM mice

To elucidate the molecular mechanism underlying the anti-inflammatory, anti-fibrotic and anti-apoptotic effect of linderalactone, RNA-Seq assay was performed. There were 699 DEGs, including 554 downregulated genes and 145 upregulated genes, between the T1DM group and control group (Fig. 3A). By comparison, the T1DM mice showed 117 downregulated DEGs and 481 upregulated DEGs in the heart tissues regardless of linderalactone treatment (Fig. 3B). Interestingly, KEGG enrichment analysis identified the potential involvement of the MAPK pathway in the activity of linderalactone in diabetic mice (Fig. 3C, D). Western blots validated that linderalactone dose-dependently inhibited the diabetes-induced upregulation of MAPKs pathway components, including p-JNK, p-Erk, and p-p38, at the protein level in heart tissues (Fig. 3E, Supplementary Fig. S1B, $P < 0.05$). Overall, 43 DEGs were upregulated in the T1DM group but downregulated in T1DM mice treated with linderalactone (Fig. 3F). These DEGs were selected for conducting a predictive analysis of transcription factors on the Enrichr website. The activating transcription factor 6B (ATF6B) ranked first, suggesting that linderalactone may mediate the activation of ATF6 in diabetic mice (Fig. 3G). Previously studies have shown the disruption of ER homoeostasis under stress conditions, such as diabetes, and a subsequent prolongation of the unfolded protein response (UPR) [18,19]. ATF6 is a key sensor protein involved in regulating ER homoeostasis [19]. As shown in Fig. 3H-J, the protein expressions of ATF6 and transcription factor C/EBP homologous protein (CHOP) were significantly increased in the T1DM group compared with the control group and that linderalactone treatment decreased the levels of ATF6 and CHOP in diabetic heart tissues ($P < 0.05$). Ultrastructural examination of the cardiac tissues revealed endoplasmic reticulum was dilated, ballooning degeneration, and fewer ribosomes in the T1DM group compared with the control group, and linderalactone overtly alleviated this abnormalitie (Fig. 3K). The above results indicate that the mechanism by which linderalactone suppresses inflammation, fibrosis and apoptosis may involve inactivation of MAPK signaling and inhibition of ATF6-mediated ER stress.

3.4. Linderalactone prevents HG-induced hypertrophy and fibrosis in cultured cardiomyocytes

Based on the promising *in vivo* protective activity of linderalactone against DCM, we wanted to determine whether linderalactone is able to inhibit the well-documented outcomes of HG (33 mM D-glucose) on cardiac cells. The effect of linderalactone on cell viability was evaluated with CCK-8 assay. As shown in Supplementary Fig. S2A, linderalactone treatment at dose from 0.2 to 125 μM had no significant effect on the viability in H9C2 cells ($P > 0.05$), but it significantly inhibited cell viability at 250 μM ($P < 0.05$). Thus, linderalactone at 10 μM and 20 μM was selected for subsequent cell experiments. RT-qPCR analysis showed that linderalactone dose-dependently suppressed the increased expression of *Anp*, *Bnp*, *Tgfb1* and *Col1* induced in H9C2 cells by HG treatment (Fig. 4A-D, $P < 0.05$). Rhodamine phalloidin staining showed that the increased cell size with HG stimulation was significantly reversed in pretreated with linderalactone (Fig. 4E, F, $P < 0.05$). In addition, linderalactone also lowered the protein expression ratio of cleaved-caspase3 to caspase3 and upregulated the level of Bcl-2 in HG-challenged H9C2 cells (Fig. 4G-I, $P < 0.05$). Apoptosis was further assessed by flow cytometry. Linderalactone treatment significantly decreased HG-induced early and late apoptotic rate in H9C2 cells (Supplementary Fig. S2B, C, $P < 0.05$). These data demonstrate that linderalactone prevents the induction of hypertrophy, fibrosis and apoptosis resulting from the HG-treatment in cardiac cells.

3.5. Linderalactone protects cardiomyocytes against HG-induced damage through inhibiting the MAPK/ATF6 signaling pathway

Since our *in vivo* results pointed to the modulation of MAPKs and ATF6 signaling pathway by linderalactone, we proceeded to determine cardiac cells under HG stimulation for such mechanism. As expected, we observed significantly increased the levels of p-JNK, p-Erk, and p-p38 with the exposure of HG, while these increases were reversed by linderalactone treatment in H9C2 cells (Fig. 5A, B, $P < 0.05$). The mRNA levels of *Tnfa* and *Il6* in HG-challenged H9C2 cells were also reduced by linderalactone (Fig. 5C, D, $P < 0.05$). To clear whether or not linderalactone-mediated anti-hypertrophic and anti-inflammatory efficiency was dependent on the activation of MAPKs, the MAPKs inhibitors mixture was used to pre-treat H9C2 cells before linderalactone treatment. The inhibition ratio of MAPKs inhibitors mixture for JNK, Erk and p38 reached 71.67%, 74.33% and 73.00% respectively (Supplementary Fig. S2D, E, $P < 0.05$). The inhibition of MAPKs remarkably reduced the cell size in HG-challenged H9C2 cells, and no additive effects were seen between HG + linderalactone group and HG + MAPKs inhibitors mixture + linderalactone group (Fig. 5E, Supplementary Fig. S2F). Consistent with this result, the mRNA levels of hypertrophy and pro-inflammatory factors with HG stimulation were inhibited by MAPKs inhibitors mixture, and there were no significant differences between HG + linderalactone group and HG + MAPKs inhibitors mixture + linderalactone group in H9C2 cells (Fig. 5F-I). Furthermore, linderalactone downregulated the expression of ATF6 in HG-challenged H9C2 cells (Fig. 6A, B, $P < 0.05$). The increased level of cytoplasmic Ca^{2+} was also prevented by linderalactone in HG-challenged H9C2 cells (Fig. 6C, Supplementary Fig. S2G, $P < 0.05$). Notably, the increased expression of ATF6 and cleaved-caspase3 with HG induction was significantly reduced by MAPKs inhibitors mixture, and it had no significant difference between HG + linderalactone group and HG + MAPKs inhibitors mixture + linderalactone group (Fig. 6D, E), indicating that no additive effects were exhibited when HG-induced cells with linderalactone and MAPKs inhibitors mixture treatment.

To strengthen our results that linderalactone preventing cardiac cells from hypertrophy and inflammation is dependent on ATF6 pathway under HG stimulation, we knocked down ATF6 in H9C2 cells, and confirmed the silencing efficiency nearly 71.0% (Fig. 6F). Importantly, knockdown of ATF6 significantly normalized HG-induced cleaved-caspase3 and Bcl-2 expression (Fig. 6G, H, $P < 0.05$). It was interesting to note that knockdown of ATF6 did not alter the levels of apoptotic-related proteins in HG-challenged cells with or without linderalactone treatment (Fig. 6G, H, $P > 0.05$). Similarly, RT-qPCR analysis showed that knockdown of ATF6 mimicked linderalactone treatment, in terms of decreasing HG-induced hypertrophic and inflammatory genes (Fig. 6I-L, $P < 0.05$), while no additive effects were displayed when ATF6-knockdown cells were pretreated with linderalactone (Fig. 6I-L, $P > 0.05$). However, knockdown of ATF6 did not influence the expression of MAPK pathway under HG stimulation (Supplementary Fig. S3), indicating that MAPK might be the upstream of ATF6. Collectively, these results suggest that the protective effect of linderalactone against HG-induced hypertrophy and inflammation may be associated with

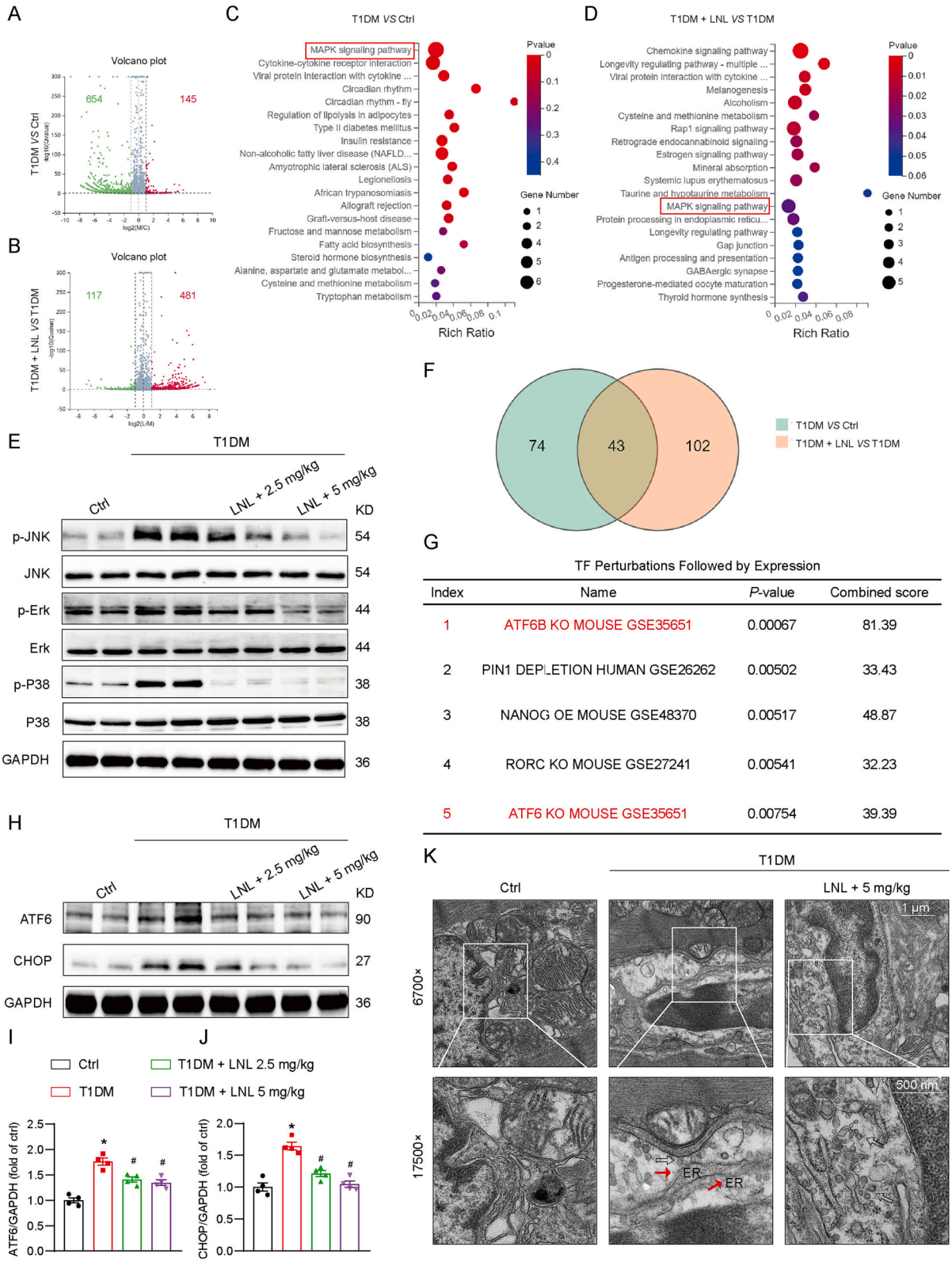

Fig. 3. Linderalactone inhibits diabetic-induced MAPKs activation and improves ATF6-mediated endoplasmic reticulum stress in T1DM mice. Five weeks after the administration of linderalactone (5 mg/kg/day), the heart was collected for *in vitro* RNA-sequencing analysis. Volcano maps showed the differentially expressed genes (DEGs) of T1DM group verses control group (A) and T1DM + LDL groups verses T1DM group (B), respectively. KEGG enrichment of upregulated DEGs in T1DM mice relative to control mice (C) and T1DM + LDL mice (D). (E) Activation of the MAPK pathway was assessed by measuring phosphorylated JNK, Erk, and p38. (F) Venn diagram of DEGs upregulated in T1DM compared to control (green), and DEGs upregulated in T1DM compared to T1DM + LDL (orange). (G) Transcription factor prediction was performed using TRRUST and ChEA3 databases. (H) Western blot assay was used to measure the protein expression levels of ATF6 and CHOP in the heart tissues of diabetic mice. Quantification of ATF6 and CHOP levels were shown in panel (I) and (J). (K) Transmission electron microscope of cardiac tissues. Red arrows indicate dilated endoplasmic reticulum; white arrows indicate ribosomes. Values are mean ± SEM, (A-D, F, G: n = 3 per group; E, H-K: n = 4 per group). $^{*}P < 0.05$ versus control; $^{\#}P < 0.05$ versus T1DM. Ctrl, control; T1DM, type 1 diabetes mellitus; LNL, linderalactone; ER, endoplasmic reticulum.

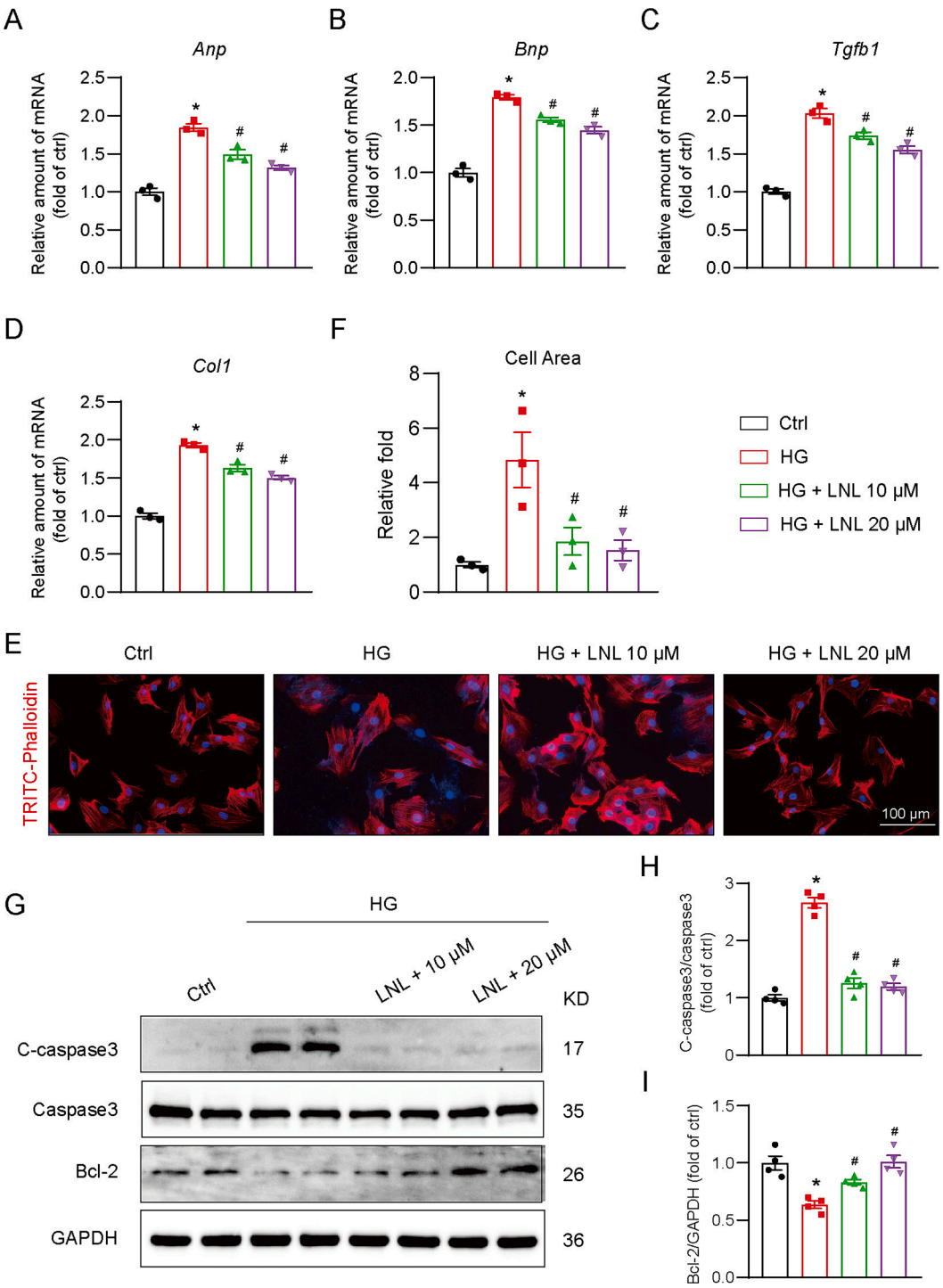

Fig. 4. Linderalactone prevents HG-induced cardiac hypertrophy, fibrosis and apoptosis in cardiac cells. H9C2 cells were pre-treated with indicated dose of linderalactone for 30 min and then incubated with HG (33 mM) for 24 h. Transcript levels of *Anp* (A), *Bnp* (B), *Tgfb1* (C) and *Col1* (D) were measured with RT-qPCR in H9C2 cells. (E) Rhodamine phalloidin staining (red) showed the effect of linderalactone on HG-induced hypertrophy in H9C2 cells. Slides were counterstained with DAPI (blue). (F) Panel showed the quantification of cell size in (E). Scale bar, 100 μm. Cell apoptotic related proteins, cleaved caspase-3 and Bcl-2 were immunoblotted in H9C2 cells (G), and quantitative analysis is shown in panel (H, I). Values are mean ± SEM, (A-F: n = 3 per group; G-I: n = 4 per group). $^{*}P < 0.05$ versus control; $^{\#}P < 0.05$ versus HG. Ctrl, control; HG, high glucose; LNL, linderalactone.

suppression of a MAPK-mediated ATF6 signaling pathway in cardiac cells.

4. Discussion

In the current study, we evaluated the cardioprotective action of linderalactone in diabetic mice. The two pivotal findings were that: (1) linderalactone significantly attenuates cardiac hypertrophy, fibrosis, and apoptosis in STZ-induced diabetic mice, possibly through modulating the MAPK-induced inflammatory response and ATF6-mediated ER stress; (2) treatment of HG-challenged cardiomyocytes with linderalactone confirmed that the protective effect involves in MAPK/ATF6-mediated inflammation and ER stress (Fig. 7). Importantly, our results revealed a mechanistic explanation for the action of linderalactone as a

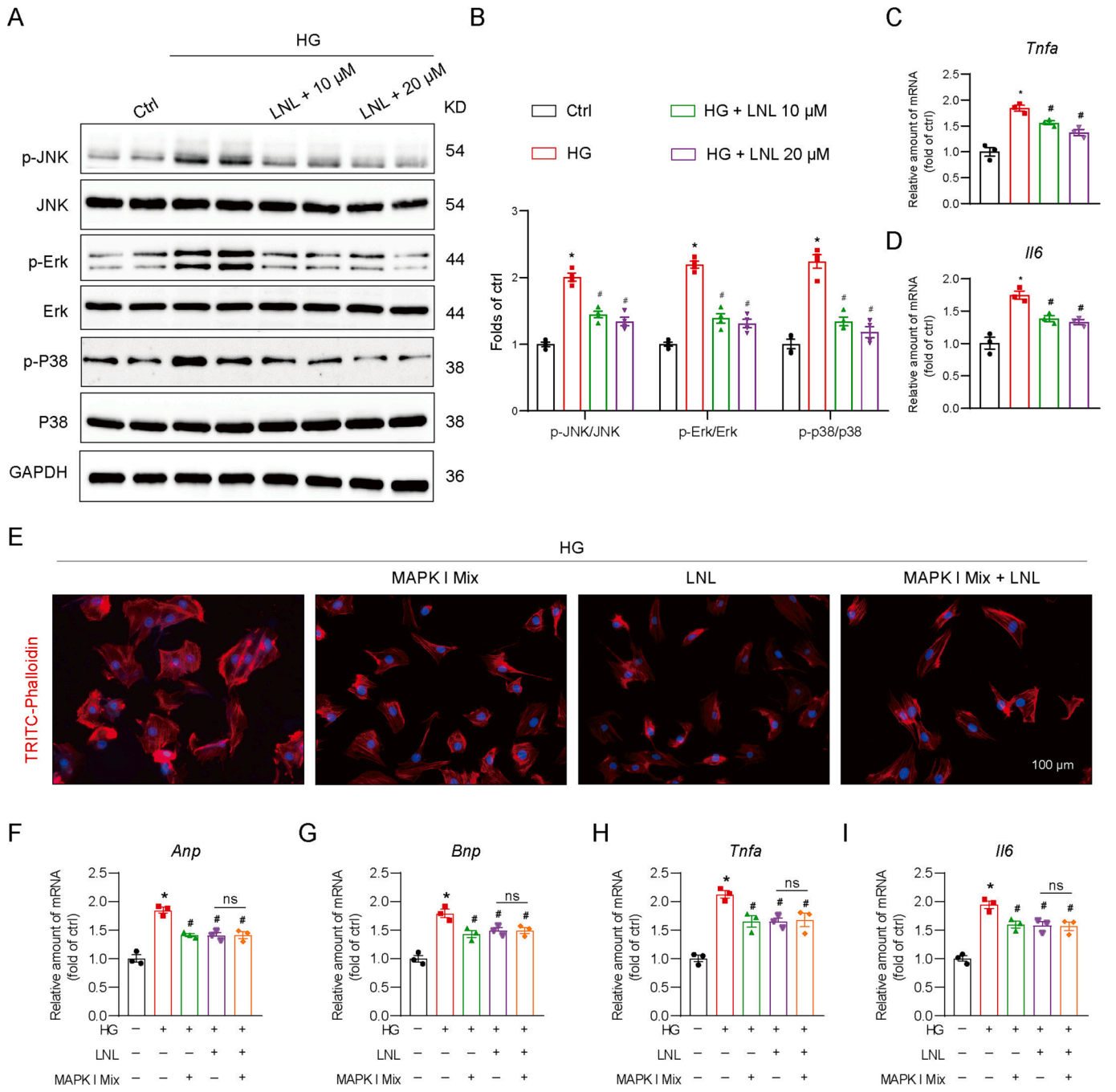

Fig. 5. Linderalactone suppresses HG-induced hypertrophy and inflammation via modulating MAPK pathway in H9C2 cells. (A) Western blot analysis showed the levels of MAPK pathway including JNK, Erk, and p38 in H9C2 cells. (B) Densitometric quantification was shown. Transcript levels of *Tnfα* (C) and *Il6* (D) were measured with RT-qPCR in H9C2 cells. H9C2 cells were pretreated with MAPK inhibitors mixture for 1 h, and then incubated with 20 μM linderalactone and 33 mM HG for 1 h. (E) Representative images of Rhodamine phalloidin staining (red) for H9C2 cells. Scale bar, 100 μm. The mRNA levels of *Anp* (F), *Bnp* (G), *Tnfα* (H), *Il6* (I) were determined. Values are mean ± SEM, (A, B: n = 4 per group; C-J: n = 3 per group). $^{*}P < 0.05$ versus control; $^{\#}P < 0.05$ versus HG. Ctrl, control; HG, high glucose; LNL, linderalactonens; ns, no significance.

potentially therapeutic candidate for preventing DCM progression.

Inflammatory responses in the myocardium are a causative factor for diabetes-induced cardiac disorders [20]. A growing number of evidence shows that pro-inflammatory factors, coupled with hypertrophy, fibrosis, and the activation of cell apoptotic pathways, play crucial roles in the progression of the biochemical, and pathological alterations related to DCM [21]. In line with previously results, the DCM in the type 1 diabetic mouse model was characterized by elevated levels of serum markers of cellular injury and increased heart hypertrophy, fibrosis, and cell death accompanied by upregulation of inflammatory factors. Similar results were observed in the HG-challenged H9C2 cells. Nevertheless, the currently available treatments for DCM remains poor.

Recent years, herbal medicines, such as sesquiterpene lactones like linderalactone, have been gathering wide attention for their cardioprotective efficacy [22,23]. Linderalactone shows extensively pharmacological potential and anticancer properties [16], but the influence of linderalactone on diabetes-associated cardiomyopathy has not been evaluated. In this study, the treatment of diabetic mice with linderalactone at either 2.5 mg/kg or 5 mg/kg showed clear protection against myocardial pathological injury and structural changes. However,

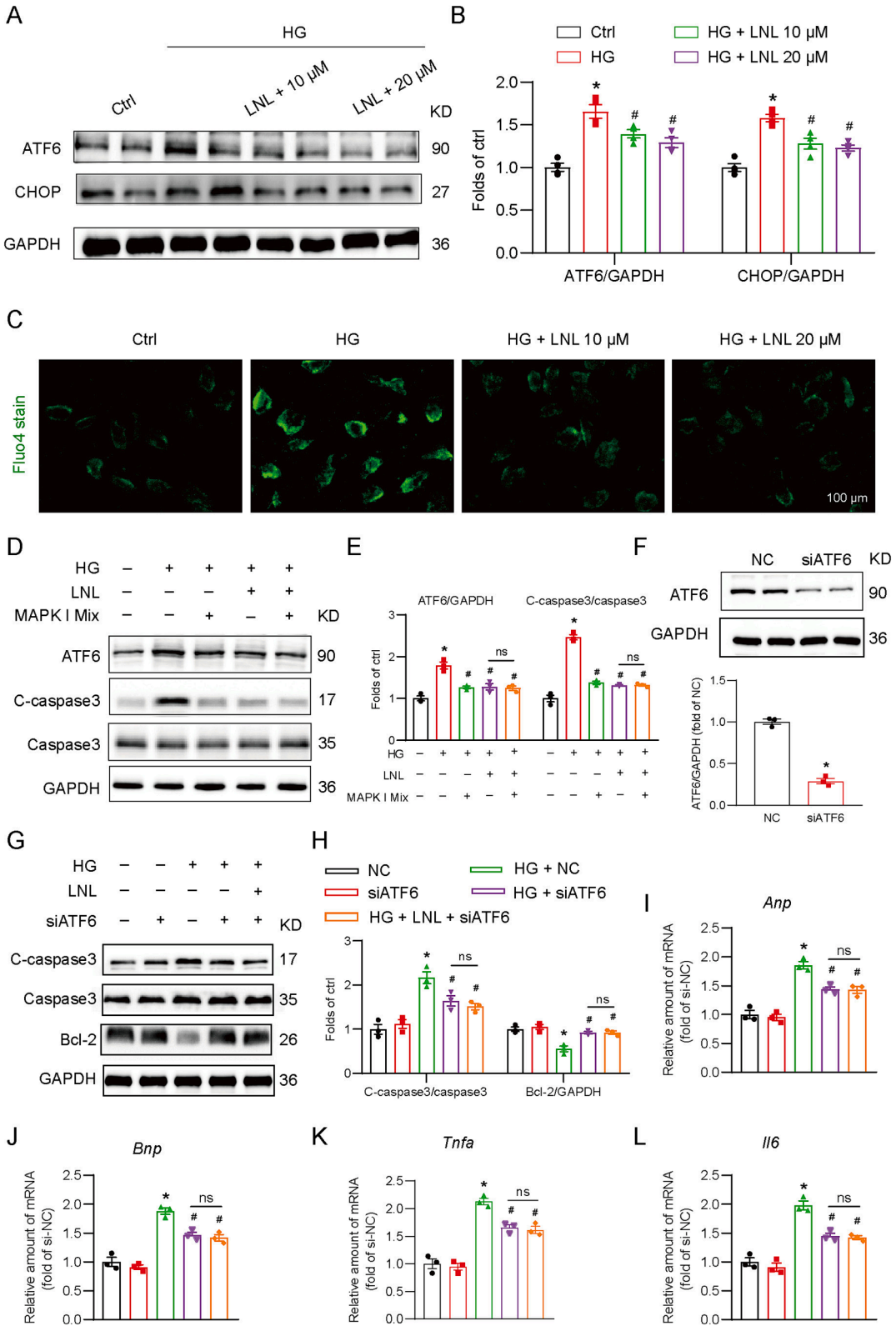

Fig. 6. Linderalactone protects cardiomyocytes against HG-induced damage through inhibiting the MAPKs/ATF6 axis. Western blot analysis of ATF6 and CHOP in the cardiac cells (A) and quantitative analysis (B). (C) Representative images of Fluo4 staining in H9C2 cells. Scale bar, 100 μm. (D) Immunoblot analysis for ATF6, cleaved caspase-3 and caspase-3 in H9C2 cells. Densitometric quantification was shown in (E). (F) Cells were transfected with negative control siRNA (NC) or siRNA against ATF6 (siATF6). Western blot analysis of ATF6 knockdown in H9C2 cells. (G) Cell lysates were probed for cleaved caspase-3, caspase-3 and Bcl-2 levels. Densitometric quantification was shown in panel (H). RT-qPCR analysis of transcript levels of *Anp* (I), *Bnp* (J), *Tnfα* (K) and *Il6* (L) in H9C2 cells. Values are mean ± SEM, (A, B, D, E: n = 4 per group; C, F-L: n = 3 per group). $^{*}P < 0.05$ versus control; $^{\#}P < 0.05$ versus HG. Ctrl, control; HG, high glucose; LNL, linderalactonens; ns, no significance.

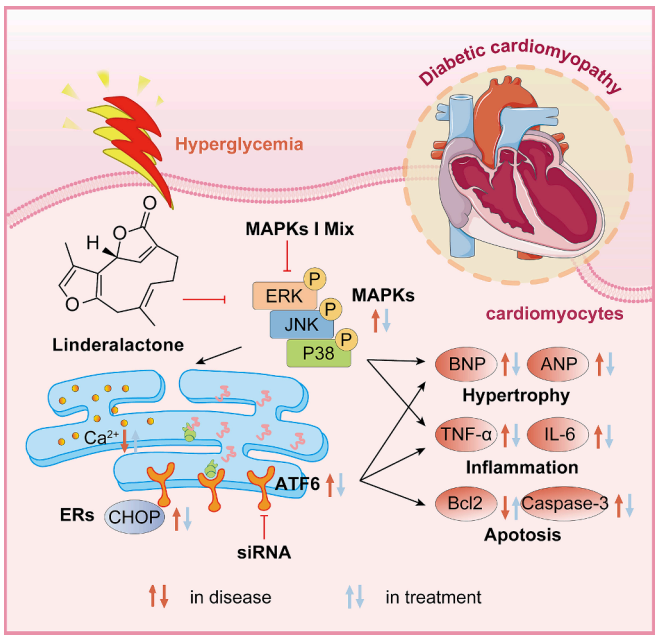

Fig. 7. The graphic illustration for the prevention of linderalactone from diabetes/HG-induced injury in cardiomyocytes.

expansion of the application of linderalactone will require exploration of its specific molecular mechanisms.

Our data from RNA-seq analysis data showed a unique involvement of the MAPK signaling pathway in the linderalactone treatment of diabetic mice. MAPKs respond to a variety of stimuli, such as cytokines, reactive oxygen species, and high glucose [24,25]. Under these stresses, highly conserved MAPK enzymes are triggered phosphorylation cascades. The MAPK signaling pathway is implicated in the pathogenesis of DCM, as the hearts of diabetic mice show upregulated phosphorylation of MAPKs. It has reported that JNK and p38 could induce the apoptosis and inflammation both in STZ-induced diabetic mice and in HG-cultured neonatal rat ventricular cardiomyocytes resulting in cardiac dysfunction [26]. Inactivation of JNK and p38 via intra-myocardial injection of lentiviruses attenuates the inflammatory response and apoptosis in diabetic mice [26]. Moreover, Erk has been reported to contribute to TGF-β expression in the condition of HG, while the upregulated TGF-β was suppressed by the Erk inhibitor U0126 [27]. Consistent with these reports, our present study demonstrated that the activation of MAPKs was robustly increased in both diabetic heart tissues and HG-induced myocardial cells, and such increases were closely associated with deterioration in myocardial hypertrophy and inflammation. Interestingly, linderalactone treatment obviously prevented the phosphorylation of MAPKs both *in vivo* and *in vitro*. Furthermore, we found that the JNK, Erk, and p38 inhibitors mixture suppressed HG-induced the increases of hypertrophic genes and inflammatory cytokines in H9C2 cells, and combining with linderalactone showed no additive effects. These results point to MAPKs as a potential therapeutic target of linderalactone for DCM.

Our further evaluations confirmed an involvement of ATF6 in the anti-DCM effects of linderalactone. The linderalactone response appears to involve ER stress, an emerging factor in chronic metabolic disorders, such as insulin resistance, obesity, and diabetes [28]. These pathological conditions destroy ER homeostasis and cause the accumulation of unfolded or misfolded proteins, resulting in a prolonged UPR and eventually causing ER stress [29]. ATF6 is a key transcriptional activator and participates in UPR signaling regulation during ER stress [30]. It has been reported that the expression of ATF6 is increased accompanied by apoptosis in hypoxia/reoxygenation (H/R)-induced myocardial cells, while knockdown of ATF6 could abolish H/R-induced cellular damage [31]. A recent study has also shown that ER stress plays a pivotal role in myocardial ischaemia/reperfusion injury in diabetic rats [32]. In this study, we found that linderalactone treatment significantly downregulated the increases in ATF6 protein levels in the diabetic myocardium and in HG-challenged H9C2 cells. The abnormal structure of the ER in the diabetic heart was also corrected by linderalactone treatment. ER stress is also implicated in pro-inflammatory signaling and pro-apoptosis by modulation of CHOP [33]. We found that linderalactone treatment decreased diabetes/HG-induced the increases expression of CHOP. It is noteworthy that ER stress causing inflammation is associated with MAPK pathway, which potentially serves as an upstream messenger for ATF6 [34,35]. ATF6 has been demonstrated to be a substrate of p38 [36]. Wang *et al.* showed that p38 could activate multiple ER sensor proteins, including CHOP, to increase the transcription activity [37]. We also found that linderalactone inhibited the HG-induced increase expression of ATF6 in H9C2 cells, and knockdown of ATF6 expression in these cells significantly improved the HG-induced apoptosis, hypertrophy, and inflammation in H9C2 cells. Collectively, these findings support the possibility that linderalactone prevents DCM in diabetic mice via actions on the MAPK/ATF6 signaling pathway.

Actually, this study had several limitations. In our experimental system, prophylactic administration was applied. To verify the possibility regarding the clinical use of linderalactone on diabetic cardiomyopathy, the therapeutic administration may be investigated in the future study. In addition, further studies will be warranted to clarify the direct target of linderalactone and illustrate the specific mechanism by which linderalactone inhibits MAPKs activation.

5. Conclusion

In summary, our study demonstrated that linderalactone possibly protected against cardiomyopathy in diabetic mice. Linderalactone has anti-hypertrophy, anti-apoptosis, and anti-inflammation activities that appears to involve inhibition of the MAPK pathway and ATF6-mediated ER stress in diabetic hearts. Along with its cardioprotective effects, linderalactone prevented HG-induced hypertrophy, apoptosis, and inflammation via MAPK/ATF6 pathway *in vitro*. Prospective research focusing on chemical analogues and combination therapy might be beneficial for the further development of linderalactone as a candidate or lead compound for the treatment of DCM. These results may provide a promising pharmaceutical alternative to address diabetes-related cardiomyopathy.

Declaration of Competing Interest

The authors declare that they have no known competing financial interests or personal relationships that could have appeared to influence the work reported in this paper.

Data availability

Data will be made available on request.

Acknowledgements

This study was supported by the National Natural Science Foundation of China (No. 31900381), the Basic Scientific Research Project of Hangzhou Medical College (Grant No. KYZD202102 and KYYB202114), and the Wenzhou City Research Project (ZY2020016).

Appendix A. Supplementary data

Supplementary data to this article can be found online at https://doi.org/10.1016/j.intimp.2023.110984.

References

[1] S.S. Jankauskas, U. Kansakar, F. Varzideh, S. Wilson, P. Mone, A. Lombardi, J. Gambardella, G. Santulli, Heart failure in diabetes, Metabolism 125 (2021), 154910.

[2] W. Wang, S. Zhang, L. Xu, Y. Feng, X. Wu, M. Zhang, Z. Yu, X. Zhou, Involvement of circHIPK3 in the pathogenesis of diabetic cardiomyopathy in mice, Diabetologia 64 (2021) 681–692.

[3] D.Z. Cherney, A. Odutayo, R. Aronson, J. Ezekowitz, J.D. Parker, Sodium glucose cotransporter-2 inhibition and cardiorenal protection: JACC review topic of the week, J. Am. Coll. Cardiol. 74 (2019) 2511–2524.

[4] Y. Tan, Z. Zhang, C. Zheng, K.A. Wintergerst, B.B. Keller, L. Cai, Mechanisms of diabetic cardiomyopathy and potential therapeutic strategies: preclinical and clinical evidence, Nat. Rev. Cardiol. 17 (2020) 585–607.

[5] G. Jia, M.A. Hill, J.R. Sowers, Diabetic cardiomyopathy: an update of mechanisms contributing to this clinical entity, Circ. Res. 122 (2018) 624–638.

[6] G. Jia, A. Whaley-Connell, J.R. Sowers, Diabetic cardiomyopathy: a hyperglycaemia- and insulin-resistance-induced heart disease, Diabetologia 61 (2018) 21–28.

[7] S.R. Savla, A.P. Laddha, Y.A. Kulkarni, Pharmacology of apocynin: a natural acetophenone, Drug Metab. Rev. 53 (2021) 542–562.

[8] M. Ruiz, L. Coderre, B.G. Allen, C. Des Rosiers, Protecting the heart through MK2 modulation, toward a role in diabetic cardiomyopathy and lipid metabolism, Biochim. Biophys. Acta Mol. Basis Dis. 1864 (2018) 1914-1922.

[9] N.T. Al-Damry, H.A. Attia, N.M. Al-Rasheed, N.M. Al-Rasheed, R.A. Mohamad, M. A. Al-Amin, N. Dizmiri, M. Atteya, Sitagliptin attenuates myocardial apoptosis via activating LKB-1/AMPK/Akt pathway and suppressing the activity of GSK-3β and p38α/MAPK in a rat model of diabetic cardiomyopathy, Biomed. Pharmacother. 107 (2018) 347–358.

[10] J. Tian, Y. Zhao, Y. Liu, Y. Liu, K. Chen, S. Lyu, Roles and mechanisms of herbal medicine for diabetic cardiomyopathy: current status and perspective, Oxid. Med. Cell. Longev. 2017 (2017) 8214541.

[11] Z. Liang, S. Leo, H. Wen, M. Ouyang, W. Jiang, K. Yang, Triptolide improves systolic function and myocardial energy metabolism of diabetic cardiomyopathy in streptozotocin-induced diabetic rats, BMC Cardiovasc. Disord. 15 (2015) 42.

[12] V. Soetikno, F.R. Sari, V. Sukumaran, A.P. Lakshmanan, S. Mito, M. Harima, R. A. Thandavarayan, K. Suzuki, M. Nagata, R. Takagi, K. Watanabe, Curcumin prevents diabetic cardiomyopathy in streptozotocin-induced diabetic rats: possible involvement of PKC-MAPK signaling pathway, Eur. J. Pharm. Sci. 47 (2012) 604–614.

[13] B. Zhang, Q. Shen, Y. Chen, R. Pan, S. Kuang, G. Liu, G. Sun, X. Sun, Myricitrin alleviates oxidative stress-induced inflammation and apoptosis and protects mice against diabetic cardiomyopathy, Sci. Rep. 7 (2017) 44239.

[14] N.A. Jani, H.M. Sirat, F. Ahmad, N.I. Aminudin, New sesquiterpene dilactone and β-carboline alkaloid and the α-glucosidase inhibitory activity of selected phytochemicals from Neolitsea cassia (L.) Kosterm, Nat. Prod. Res. 36 (2022) 4061–4069.

[15] J.H. Park, M.J. Kim, W.J. Kim, K.-D. Kwon, K.-T. Ha, B.T. Choi, S.-Y. Lee, H.K. Shin, Isolinderalactone suppresses human glioblastoma growth and angiogenic activity in 3D microfluidic chip and in vivo mouse models, Cancer Lett. 478 (2020) 71–81.

[16] Y. Deng, Y. Li, Linderalactone inhibits human lung cancer growth by modulating the expression of apoptosis-related proteins, G2/M cell cycle arrest and inhibition of JAK/STAT signalling pathway, J. B.U.ON. 24 (2019) 566–571.

[17] X. Han, J. Zhang, L. Zhou, J. Wei, Y. Tu, Q. Shi, Y. Zhang, J. Ren, Y. Wang, H. Ying, G. Liang, Sclareol ameliorates hyperglycemia-induced renal injury through inhibiting the MAPK/NF-κB signaling pathway, Phytother. Res. 36 (2022) 2511–2523.

[18] J. Ren, Y. Bi, J.R. Sowers, C. Hetz, Y. Zhang, Endoplasmic reticulum stress and unfolded protein response in cardiovascular diseases, Nat. Rev. Cardiol. 18 (2021) 499–521.

[19] Y.-F. Yang, H. Wang, N. Song, Y.-H. Jiang, J. Zhang, X.-W. Meng, X.-M. Feng, H. Liu, K. Peng, F.-H. Ji, Dexmedetomidine attenuates ischemia/reperfusion-induced myocardial inflammation and apoptosis through inhibiting endoplasmic reticulum stress signaling, J. Inflamm. Res. 14 (2021) 1217–1233.

[20] M.H. Abukhalil, O.Y. Althunibat, S.H. Aladaileh, W. Al-Amarat, H.M. Obeidat, A.-A.-M.-A. Al-Khawalde, O.E. Hussein, M.A. Alfwuaires, A.I. Algefare, K.M. Alanazi, F.K. Al-Swailmi, H.H. Arab, A.M. Mahmoud, Galangin attenuates diabetic cardiomyopathy through modulating oxidative stress, inflammation and apoptosis in rats, Biomed. Pharmacother. 138 (2021), 111410.

[21] M.-X. Zhao, B. Zhou, L. Ling, X.-Q. Xiong, F. Zhang, Q. Chen, Y.-H. Li, Y.-M. Kang, G.-Q. Zhu, Salusin-β contributes to oxidative stress and inflammation in diabetic cardiomyopathy, Cell Death Dis. 8 (2017) e2690.

[22] R. Gimenes, C. Gimenes, C.M. Rosa, N.P. Xavier, D.H.S. Campos, A.A.H. Fernandes, M.D.M. Cezar, G.N. Guirado, L.U. Pagan, I.D. Chaer, D.C. Fernandes, F.R. Laurindo, A.C. Cicogna, M.P. Okoshi, K. Okoshi, Influence of apocynin on cardiac remodeling in rats with streptozotocin-induced diabetes mellitus, Cardiovasc. Diabetol. 17 (2018) 15.

[23] S. Shabab, Z. Gholamnezhad, M. Mahmoudabady, Protective effects of medicinal plant against diabetes induced cardiac disorder: A review, J. Ethnopharmacol. 265 (2021), 113328.

[24] S. Wang, L. Ding, H. Ji, Z. Xu, Q. Liu, Y. Zheng, The role of p38 MAPK in the development of diabetic cardiomyopathy, Int. J. Mol. Sci. 17 (2016).

[25] Z. Xu, J. Sun, Q. Tong, Q. Lin, L. Qian, Y. Park, Y. Zheng, The role of ERK1/2 in the development of diabetic cardiomyopathy, Int. J. Mol. Sci. 17 (2016).

[26] G. Zuo, X. Ren, X. Qian, P. Ye, J. Luo, X. Gao, J. Zhang, S. Chen, Inhibition of JNK and p38 MAPK-mediated inflammation and apoptosis by ivabradine improves cardiac function in streptozotocin-induced diabetic cardiomyopathy, J. Cell. Physiol. 234 (2019) 1925–1936.

[27] H. Wu, G.-N. Li, J. Xie, R. Li, Q.-H. Chen, J.-Z. Chen, Z.-H. Wei, L.-N. Kang, B. Xu, Resveratrol ameliorates myocardial fibrosis by inhibiting ROS/ERK/TGF-β/periostin pathway in STZ-induced diabetic mice, BMC Cardiovasc. Disord. 16 (2016) 5.

[28] I.L. Lemmer, N. Willemsen, N. Hilal, A. Bartelt, A guide to understanding endoplasmic reticulum stress in metabolic disorders, Mol Metab 47 (2021), 101169.

[29] J. Lu, Q.-M. Dai, G.-S. Ma, Y.-H. Zhu, B. Chen, B. Li, Y.-Y. Yao, Erythropoietin attenuates cardiac dysfunction in rats by inhibiting endoplasmic reticulum stress-induced diabetic cardiomyopathy, Cardiovasc. Drugs Ther. 31 (2017) 367–379.

[30] N. Nasiri-Ansari, C. Nikolopoulou, K. Papoutsi, I. Kyrou, C.S. Mantzoros, G. Kyriakopoulos, A. Chatzigeorgiou, V. Kalotychou, M.S. Randeva, K. Chatha, K. Kontzoglou, G. Kaltsas, A.G. Papavassiliou, H.S. Randeva, E. Kassi, Empagliflozin attenuates non-alcoholic fatty liver disease (NAFLD) in high fat diet fed ApoE(-/-) mice by activating autophagy and reducing ER stress and apoptosis, Int. J. Mol. Sci. 22 (2021).

[31] J.-Y. Tang, P. Jin, Q. He, L.-H. Lu, J.-P. Ma, W.-L. Gao, H.-P. Bai, J. Yang, Naringenin ameliorates hypoxia/reoxygenation-induced endoplasmic reticulum stress-mediated apoptosis in H9c2 myocardial cells: involvement in ATF6, IRE1α and PERK signaling activation, Mol. Cell. Biochem. 424 (2017) 111–122.

[32] J. Li, Y. Zhao, N. Zhou, L. Li, K. Li, Dexmedetomidine attenuates myocardial ischemia-reperfusion injury in diabetes mellitus by inhibiting endoplasmic reticulum stress, J. Diabetes Res. 2019 (2019) 7869318.

[33] Y. Zhong, C. Jin, J. Han, J. Zhu, Q. Liu, D. Sun, X. Xia, X. Peng, Inhibition of ER stress attenuates kidney injury and apoptosis induced by 3-MCPD via regulating mitochondrial fission/fusion and Ca2+ homeostasis, Cell Biol. Toxicol. 37 (2021) 795–809.

[34] D.J. Thuerauf, N.D. Arnold, D. Zechner, D.S. Hanford, K.M. DeMartin, P. M. McDonough, R. Prywes, C.c., Glembotski, p38 Mitogen-activated protein kinase mediates the transcriptional induction of the atrial natriuretic factor gene through a serum response element. A potential role for the transcription factor ATF6, J. Biol. Chem. (1998) 273, pp. 20636–20643.

[35] B. Xu, J. Xu, N. Cai, M. Li, L. Liu, Y. Qin, X. Li, H. Wang, Roflumilast prevents ischemic stroke-induced neuronal damage by restricting GSK3β-mediated oxidative stress and IRE1α/TRAF2/JNK pathway, Free Radic. Biol. Med. 163 (2021) 281–296.

[36] S. Luo, A.S. Lee, Requirement of the p38 mitogen-activated protein kinase signalling pathway for the induction of the 78 kDa glucose-regulated protein/immunoglobulin heavy-chain binding protein by azetidine stress: activating transcription factor 6 as a target for stress-induced phosphorylation, Biochem. J 366 (2002) 787–795.

[37] X.Z. Wang, D. Ron, Stress-induced phosphorylation and activation of the transcription factor CHOP (GADD153) by p38 MAP Kinase, Science 272 (1996) 1347–1349.